

pubs.acs.org/JPCA Article

Flow-Optimized Model for Gas Jet Desorption Sampling Mass Spectrometry

Xi Chen, G. Asher Newsome,* Michael Buchanan, Jeremy Glasper, Leyan Hua, Mohsen Latif, Viraj Gandhi, Xintong Li, and Carlos Larriba-Andaluz*



Cite This: J. Phys. Chem. A 2023, 127, 1353–1359



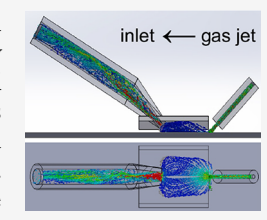
ACCESS I

III Metrics & More

Article Recommendations

Supporting Information

ABSTRACT: Thermal gas jet probes, including post-plasma desorption/ionization sources, have not been studied using computational fluid dynamics (CFD) models, as have other ambient mass spectrometry sampling techniques. Two systems were constructed: a heated nitrogen jet probe to establish practical bounds for a sampling/transmission experiment and a CFD model to study trajectories of particles desorbed from a surface through optimization of streamlines and temperatures. The physical model configuration as tested using CFD revealed large losses, transmitting less than 10% of desorbed particles. Different distances between the desorption probe and the transport tube and from the sample surface were studied. The transmission improved when the system was very close to the sample, because the gas jet



otherwise creates a region of low pressure that guides the streamlines below the inlet. A baffle positioned to increase pressure in the sample region improves collection efficiency. A Lagrangian particle tracking approach confirms the optimal design leading to a transmission of almost 100%.

INTRODUCTION

The numerous methods of ambient sampling for mass spectrometry (MS) are adept at desorbing surface organic molecules from bulk materials using gas streams, condensedphase flow, or laser heating. Desorption electrospray ionization (DESI)¹ and direct analysis in real time (DART)² were the first of these techniques, but more variants on a post-plasma gas probe like DART have been developed since.^{3,4} Localized surface heating is the major driver of the desorption process with post-plasma probes. However, ionization need not be immediate upon analytes entering the gas phase. Because analyte as a neutral aerosol or gas is transported more easily than ions through a field-free, atmospheric pressure tube leading to a mass spectrometer, 5,6 there are advantages to decoupling desorption from ionization such as accessing analytes far from the instrument. Tools like the iKnife⁷ and lasers⁸ can vaporize the sample for later ionization, but a jet of heated neutral gas is cheaper and more accessible. Jets of simple nitrogen or solvent vapor 10,11 can be oriented in any way including transmission mode, but surface-sampling techniques including conventional DART direct a gas jet at an acute angle to the broad face of an object. 12-15

A gas jet directed at a planar macroscopic object turbulently flows along the surface until it is inefficiently collected into an MS vacuum inlet or a transport tube, as shown by Schlieren imaging. Computational fluid dynamics (CFD) have been used to model the desorption and transfer process for DESI^{17,18} and to make laser ablation electrospray ionization more efficient, but only empirical two-dimensional effects of planar surface desorption have been studied for thermal jet sampling. The development of DART and other gas

probes has focused on design elements to reduce probe cost, ^{22–24} pursue alternative chemistries, ^{10,25–27} minimize thermal effects, ²⁸ or use alternative plasma gas. ^{26,29–31} Instead of relying on advantageous chemistry alone to maximize analyte signal in mass spectra, this research uses CFD to model gas jet thermal desorption from a planar surface to improve efficiency for surface sampling. The model presented here does not simulate a DART probe specifically but generalizes the system to neutral thermal jet desorption to study flow dynamics absent of charge.

METHODS

Physical Model. To create a framework for the CFD simulation relevant to effective MS, a physical desorption system capable of adjusting each of the involved variables was built first. A heated neutral gas probe was constructed from concentric tubing connected to a nitrogen supply. The probe consisted of 0.89 mm id, 1.59 mm od copper tubing; jacketed by 1.60 mm id, 3.18 mm od alumina tubing; wrapped with a 2.84 g (approximately 1 m) coil of 22-gauge Nichrome wire; and with an outer jacket of 4.77 mm id, 6.35 mm od alumina tubing. The core copper tubing was positioned so that upon thermal expansion it would be flush to the inner alumina tubing. A k-type thermocouple was fixed at 2.5 cm from the probe end with

Received: November 14, 2022 Revised: January 12, 2023 Published: January 26, 2023





fiberglass tape (Figure S1). The probe body was mounted from above at 45° to normal. Nitrogen was supplied at rates set by a Masterflex mass flow controller (Cole-Parmer, Vernon Hills, IL). The probe and continuously flowing gas were heated by a 15.5 V supply to the Nichrome coil, regulated by a temperature controller according to thermocouple feedback. An Arduinooperated shutter vane¹⁵ was positioned below the probe to control sample surface exposure, opening for 5 s at a time for discrete thermal desorption experiments. To collect desorbed materials, 2 m stainless steel tubing with 6.35 mm od and 3.8 mm id heated to 150 °C (Clayborn Lab, Truckee, CA) was mounted opposite to the gas probe, 45° to normal to accommodate a wide sample surface. The rear of the conduit was connected to a tee with a custom-mounted DART probe and a supplementally pumped Vapur inlet (IonSense, Saugus, MA) (Figure S2). The 1/2" DART cap is sealed into the reaction tee with the O-ring of an Ultra-Torr fitting. Materials transported from the desorption site were ionized within the reaction tee using DART helium set to the minimum 50 °C to ensure reproducibility. Transport tube speeds determined by the supplemental pump were measured with a Defender 510 piston flow meter (MesaLabs, Lakewood, CO). Ions were detected by an LTQ Orbitrap Velos mass spectrometer (Thermo Fisher, Waltham, MA) at 30 k resolving power.

Simulated Desorption Space. A model of the neutral desorption/sampling area was generated through a parametric feature-based approach using computer-aided design (CAD) software, SOLIDWORKS (version 2017 SP0, Waltham, MA), according to the physical dimensions and empirically optimized settings for the physical system. The design was based on the model, including the outlet desorption tube (source of the nitrogen jet), simplified inlet tube (entrance to transport tubing), and sample plate. The flow simulations for the system were performed using the CFD package to analyze the flow inside the desorption system using finite volume methods for the flow simulation according to the conservation law of flow properties (i.e., mass, momentum, and energy). A series of hexahedral meshes were generated for the fluid domain based on the geometric construction. Dynamic meshing was processed automatically during the calculation progress, refining the flow domain where sudden change of flow property occurs to improve the accuracy, as well as roughing the meshes where the gradients of flow property of contiguous grids are negligible, in order to enhance computational efficiency. As such, the mesh was refined close to the tubes and the surface of the sample plate while getting rougher near the upper portion of the fluid domain. The refining was stopped when little to no difference was observed between two consecutive refinements. The initial model and a comparison of the two final refined meshes are shown in Figures S3 and S4 with the corresponding comparison of results at the center plane.

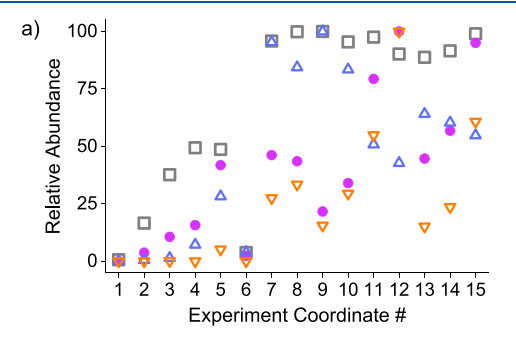
Laminar and turbulence models were selected for the gas flow simulation. For the turbulence model, Favre-averaged Navier—Stokes equations were used, which incorporate time-averaged effects of turbulence perturbations. When these equations are employed, transport equations are used to describe the turbulent kinetic energy and its dissipation rate, which is known as the $k-\varepsilon$ model. For boundary conditions, the experimental flow rates of 1.2 and 0.2 L/min were applied for inlet and probe tubes, respectively. Temperatures of 423, 473, and 293 K were applied on the inlet tube, outlet tube, and sample plate, respectively. Once the simulation converged (300–400 iterations) and a steady state was reached, the velocity profile, streamlines coming

out of the outlet, streamlines going into the inlet, and the temperature profile are recorded. Lagrangian tracking of 1000 spherical particles with a diameter of 0.1–1 nm initially placed on the plate at the impinging location of the heated desorbing flow was used to mimic the sample particles' trajectory under the flow field.

The original system was subsequently modified to improve sensitivity based on previous iterations starting with the initial model above. Distance from the substrate, distance between tubes, and the shape of the sampling were studied. To increase pressure in the desorbing region, a baffle was placed above the tubes and its effect optimized.

RESULTS AND DISCUSSION

Empirical Optimization of the Physical Model. Thermal paper was used to characterize neutral heated gas jet interaction



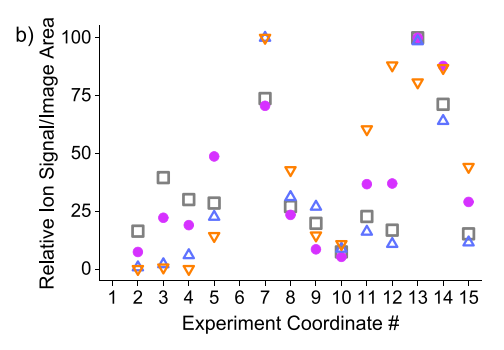


Figure 1. Relative signal abundance (a) and signal compared to measured impact area (b) for diphenyl sulfone (gray \square), $[C_{14}H_{13}O]^+$ (pink \blacksquare), bisphenol S (blue \triangle), and $[C_{17}H_{32}NO_6]^+$ (orange ∇) from various settings and configurations.

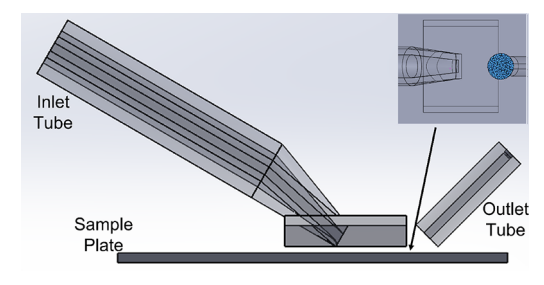


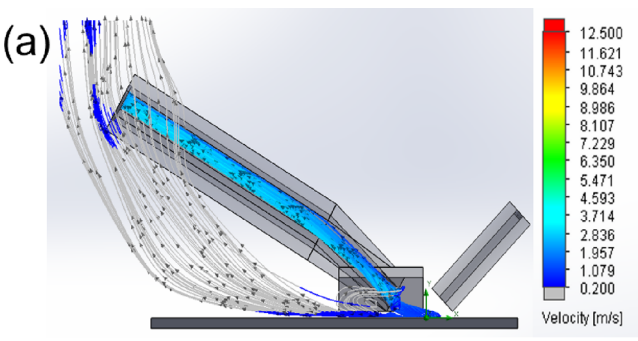
Figure 2. Sketch of the thermal desorption system and the zoomed-in position of the particles that were used for the post-process.

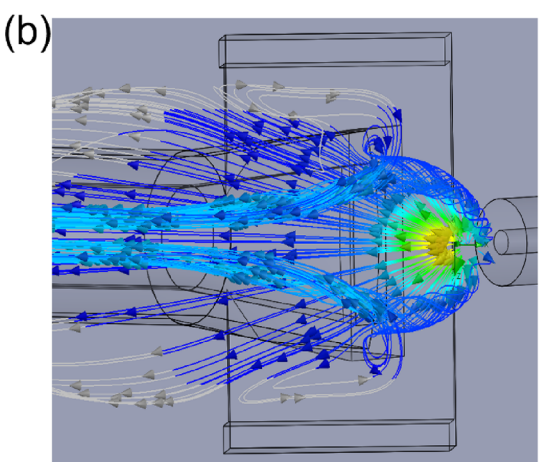
with a flat surface in the physical model. The thermochromic dyes developing on the paper provided a visual recording of the impact area, and multiple compounds desorbed from the paper contributed to the MS signal. The ion signal from thermal desorption of four representative analytes varying up to 200-fold

Table 1. Transmission Efficiency for Different Cases Studied a

	without baffle			with baffle		
distance between tubes (mm)	4	7	11	4	7	11
1.8 mm ² nozzle area transmission efficiency	59.5	27.3	25.1	70.9	99.9	100
13.7 mm ² nozzle area transmission efficiency	54.8	24.5	22.3	62.3	77.7	93.3

[&]quot;The distance to the sample plate was kept at 0.635 mm for all cases presented in the table.





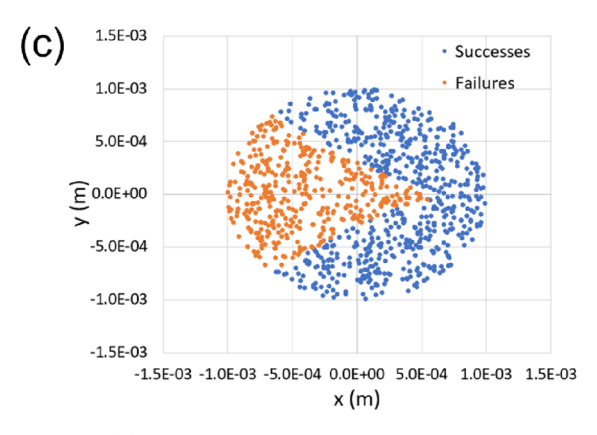


Figure 3. (a) Front view of the particles' trajectory with an inlet/probe distance of 3 mm; the streamlines were marked as gray when the velocity magnitude is less than 0.2 m/s. (b) Top view of the particles' trajectory. (c) Fates of the 1000 particles. In the orange fan area where the particles failed to enter the inlet tube, the rest of the particles, which were marked in blue color, successfully went into the inlet tube. The x and y axes are given in meters.

absolute abundance (Figure S5) was tracked to compare experimental configurations. Signal and impact area were a product of a complex relationship between the position of the gas probe relative to the inlet, the heated nitrogen jet flow rate, and the transfer tube inlet suction rate; each setting was adjusted to yield different surface impact areas (Figure 1a). The four analyte ions did not necessarily have the same abundance relative to each other using each configuration. The signal was consistently improved by minimizing the transport tube inlet speed from experiments #1-5 (Table S1), similar to other results with a DART ion source and a conventional 40 mm transport tube.³² The measured inlet speed represents the net suction on desorbed analytes after supplemental pumping removes the majority of the DART helium flow. The minimum supplemental pump speed necessary to maintain nominal ion trap vacuum produced an inlet suction of 1.2 L/min. Inlet speeds below 4 L/min produced greater single-spectrum abundance but also more analyte spread within the transport tubing, such that the signal could linger for tens of seconds or longer beyond the desorption window. The supplemental pump speed was pulsed higher between experiments to prevent carryover.

The system configuration was further tuned to adjust the impact area dimensions. Millimeter changes to the gas jet distance from the inlet produced minor signal improvement. The gas jet speed had a significant effect, but the ion signal did not increase linearly with the jet speed. Correcting the ion signal magnitude for the size of the impact area (Figure 1b) demonstrated that the process of collecting desorbed analytes into the transport tube inlet determines the effectiveness of the experiment. The sampling configurations that produced the maximum average abundance in Figure 1a, #12 or 15, were not identical to the settings that produced the most signal per desorption area in Figure 1b, #7 or 13.

Simulation and CFD Model Optimization. The CFD model system was built in simulation space to study the factors that affect desorbed material capture efficiency within the constraints discovered using the optimized physical system, such as the capture area of the sample nozzle, distance between inlet and outlet tubes, distance to the substrate, and pressure differential within the system. A typical model is shown in Figure 2. In Figure 2, the inlet tube was set to 423 K with 3.8 mm id and 6.35 mm od, and the suction rate was fixed at 1.2 L/min. The temperature of the probe tube was set at 473 K with 0.89 mm id and 3.18 mm od, with a nitrogen fluid at a flow rate of 0.2 L/min. The sample plate was set to 293 K for all simulations; although it would be warmed a finite amount by the hot nitrogen pulse, it was set to a constant temperature rather than approximate the spread (greatly exceeded by the duration of the jet) through samples of unknown thermal conductivity. The tubes were 45° from the horizontal surface and 0.635-2.54 mm distance away from the sample plate. The Figure 2 inset shows the position of a set of 1000 spherical particles of 0.1-1 nm in size randomly placed within a 2 mm circle. The particles were used to mimic the desorbed molecules entering the inlet tube. The sample tube flow area at the nozzle was varied between 1.767 and 13.7 mm². The different nozzles tested are shown in Figure S6. The distance between desorbing and sampling tubes was also varied between 4 and 11 mm. Finally, the system was tested with and without a staple-shaped baffle to modify the pressure in the sample region. The baffle has two sidewalls and no rear wall, positioning the top of the baffle 2.73 mm above the bottommost part of the inlet.

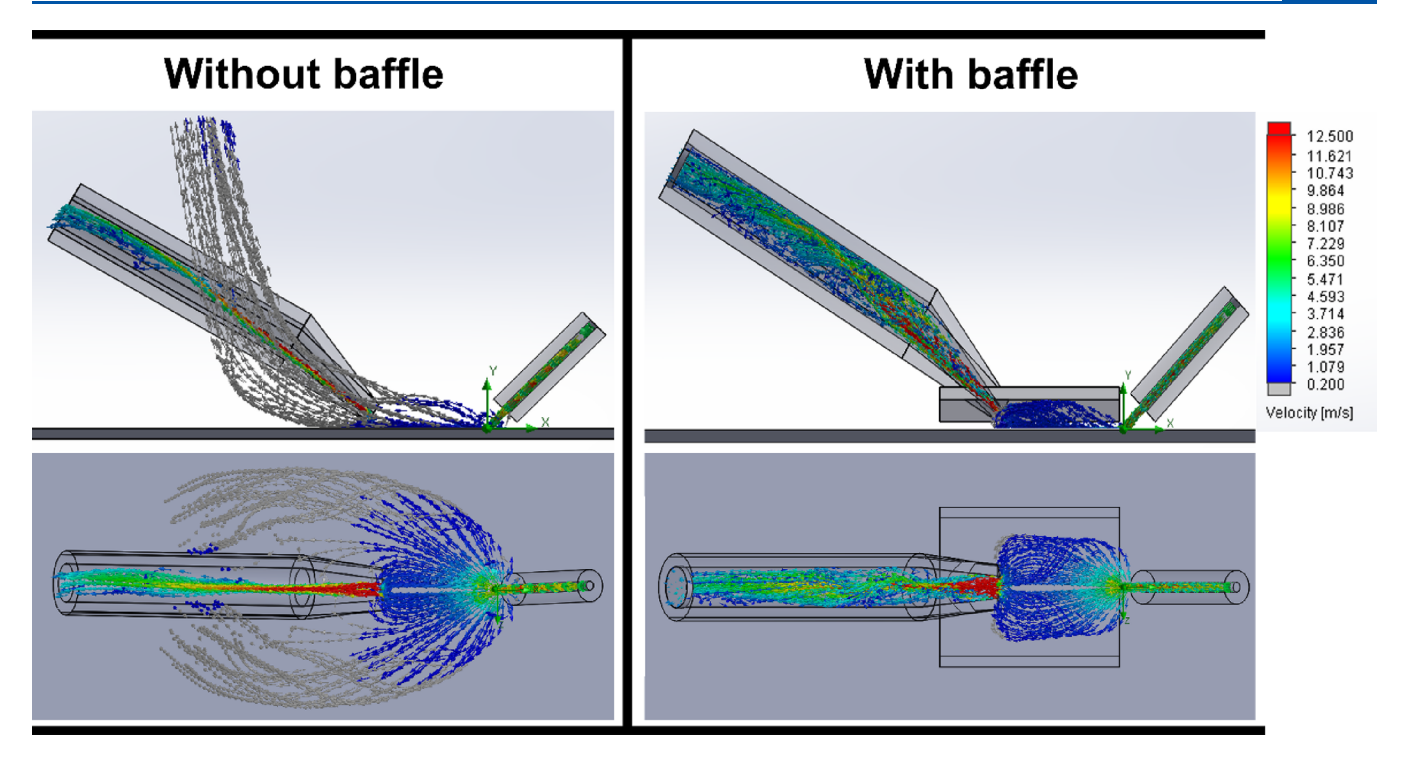


Figure 4. Comparison of particles' trajectory with and without a baffle. Front and top views were used of a small nozzle with a distance of the inlet/outlet tube at 11 mm.

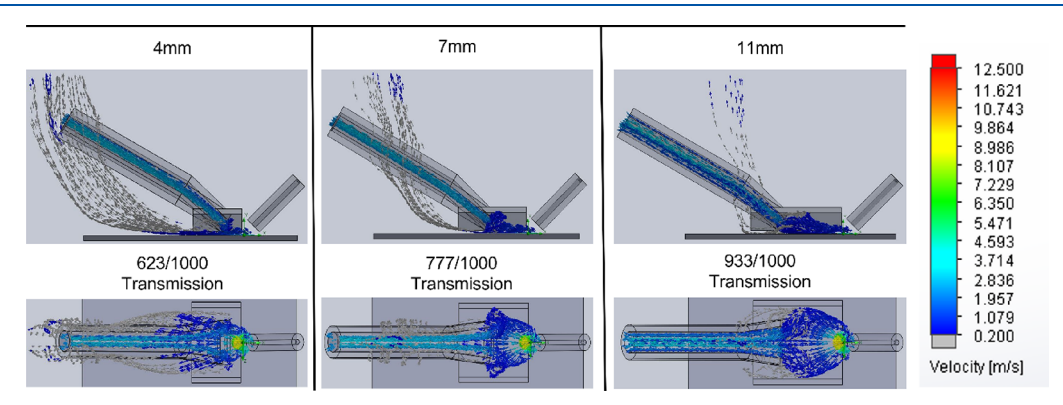


Figure 5. Front and top views of the particles' trajectory of a small nozzle (the open area is 13.7 mm²) with a distance of the inlet/outlet tube at 4, 7, and 11 mm, respectively.

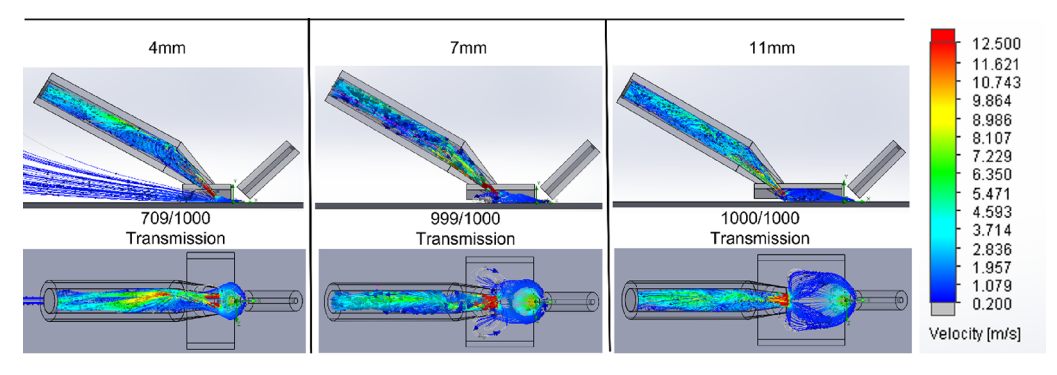


Figure 6. Front and top views of the particles' trajectory of a small nozzle (the open area is 1.8 mm²) with a distance of the inlet/outlet tube at 4, 7, and 11 mm, respectively.

Table 1 shows a summary of the results based on the transmission of desorbed particles for the most optimal cases. In what follows, an abridged precis, explanation, and motivation for the changes are provided. Initial testing showed negligible

transmission at 2.54 mm, so only the 0.635 mm case was fully optimized. The reason for negligible transmission was due to most of the desorbing tube streamlines flowing under the sampling tube, as observed in Figure S7. Regarding the tube

nozzle flow area, the smaller flow area nozzle (1.767 mm²) had the highest transmission. The underlying cause seems to be that increasing velocity (due to the flow rate being constant between the nozzles) results in a reduced pressure area and an increase in the suction of the immediately surrounding streamlines, akin to what occurs under Bernoulli's principle for inviscid flow. Due to the reduced pressure area, the streamlines being sucked come from gas above the system (Figure S8), and therefore, the nozzle area without a baffle has a negligible effect on transmission. The baffle was incorporated to reduce the pressure in the sampling region, slowing down the flow close to the sample tube so that the analytes can be sucked into the system. Figure S8 provides the post-processed results of the streamlines that make it to the sample tube mostly come from surrounding air due to the drop in pressure near the sampling region. The baffle would serve to reduce the pressure and recircle the streamlines, increasing transmission. Finally, while the sample tube angle was modified (Figure S6), its effect on transmission was negligible.

A typical result of the study of transmission for one particular configuration is shown in Figure 3. Figure 3a,b shows the side and top views of the system for a large nozzle (the open area is 13.7 mm²) with 4 mm being the distance between the two tubes in this case. The figures show the particles' trajectory coming out of the desorbing region. The baffle helps recirculate the air flow underneath it, allowing more particles along with the air flow to be pulled into the inlet. Figure 3c shows the position of the desorbed particles that made it inside the inlet. Based on the statistical study, 623 out of 1000 particles were detected that successfully entered into the inlet tube. As observed in Figure 3c, there is a fan area, marked in orange where particles failed to be sampled, and where a mixture of close position to the sample tube and high velocity is responsible for the loss. In contrast, the particles in the blue section recirculated under the baffle and successfully entered the inlet tube, as depicted in Figure 3b.

The effect of the baffle on the particle trajectory is shown in Figure 4, where the simulation with an inlet/probe tube distance of 11 mm was run with and without the baffle. Without the baffle, most of the particles flow below and to the sides of the sampling tube and were dispersed to the background environment. The transmission efficiency is 25.1%. Positioning the baffle above the tubes helps with the recirculation of the particles, preventing the suction effect and substantially increasing the transmission. The result is immediately visible where the transmission efficiency in this case increases to almost 100%.

To finalize the optimization, one would like to study the effect of varying the distance between the inlet and outlet tubes with a baffle. The nozzle area was kept at the largest value (13.7 mm²) while increasing the distance between the inlet and outlet tubes from 4 to 7 and 11 mm. The baffle was stretched as the distance increased. As can be observed in Figure 5, the transmission efficiency was increased from 62.3 to 77.7 and 93.3%, respectively.

The open area of the nozzle of the inlet tube also plays an important role that affects the flow field. Figure 6 shows the side and top views of the particles' trajectory at the same metrics of distance as in Figure 5, while the open area was reduced from 13.7 to 1.8 mm². With the same flow rate, the smaller open area of the nozzle corresponds to a higher initial velocity, which created a lower pressure zone to push more particles into the inlet tube. At a 4 mm distance, there were still some particles that failed to enter the inlet tube, due to the high initial velocity from the probe, and the transmission efficiency lowered to 70.9%.

When the distance was extended to 7 and 11 mm, the velocity of the ions recirculated and slowed down under the baffle, almost all of the particles could be pulled into the inlet probe, and the transmission efficiency is close to 100%.

CONCLUSIONS

The numerous factors affecting the efficiency of a thermal jet desorption and suction/transport system are ultimately too many and too inter-related to be fully explored through empirical optimization. Modeling a desorption system under a small set of constraints known to be conducive to ionization provided a more direct measure of sampling efficiency, trading experiment time for computation power. The finding that most of the fluid transmitted through a suction inlet comes from the surroundings, though a flowing source is directly across from said inlet, is a significant addition to the Schlieren imaging observation that a thermal jet angled toward a plane does not "bounce" but flows along the surface. The above-inlet baffle design created here could well be used to improve other thermal jet desorption sources such as DART operated in a surface mode.

Independent of the efficiency with which an inlet collects desorbed materials, there are other practical considerations for using a gas jet sampling system to analyze surfaces on real objects. The submillimeter positioning for optimal sampling requires mounting both the gas probe/inlet and the sample itself in some stable configuration, with the positioning of at least one of them controlled by micrometers. The logistical difficulty is compounded for particularly large or weighty samples. Conversely, small surfaces may be more difficult to accommodate with the gas probe as much as a centimeter from the inlet. Such factors will be explored in future studies.

ASSOCIATED CONTENT

Supporting Information

The Supporting Information is available free of charge at https://pubs.acs.org/doi/10.1021/acs.jpca.2c07999.

Gas jet probe configuration; ion source configuration; meshing of initial CFD configuration; streamline from initial CFD configuration; mass spectrum from physical model sampling; settings for the physical model; sample nozzles for CFD; streamline flow under the sampling tube; and streamlines from surrounding air (PDF)

AUTHOR INFORMATION

Corresponding Authors

G. Asher Newsome — Smithsonian Museum Conservation Institute, Suitland, Maryland 20746, United States; orcid.org/0000-0003-1683-2197; Phone: 301-238-1223; Email: newsomeg@si.edu

Carlos Larriba-Andaluz — Department of Mechanical and Energy Engineering, IUPUI, Indianapolis, Indiana 46202, United States; ⊚ orcid.org/0000-0003-0864-7733; Phone: 317-274-8993; Email: clarriba@iupui.edu

Authors

Xi Chen — Department of Mechanical and Energy Engineering, IUPUI, Indianapolis, Indiana 46202, United States; Department of Mechanical Engineering, Purdue University, West Lafayette, Indiana 47907, United States

- Michael Buchanan Department of Mechanical and Energy Engineering, IUPUI, Indianapolis, Indiana 46202, United States
- Jeremy Glasper Department of Mechanical and Energy Engineering, IUPUI, Indianapolis, Indiana 46202, United States
- Leyan Hua Department of Mechanical and Energy Engineering, IUPUI, Indianapolis, Indiana 46202, United States
- Mohsen Latif Department of Mechanical and Energy Engineering, IUPUI, Indianapolis, Indiana 46202, United States
- Viraj Gandhi Department of Mechanical and Energy Engineering, IUPUI, Indianapolis, Indiana 46202, United States; Department of Mechanical Engineering, Purdue University, West Lafayette, Indiana 47907, United States
- Xintong Li Department of Mechanical and Energy Engineering, IUPUI, Indianapolis, Indiana 46202, United States

Complete contact information is available at: https://pubs.acs.org/10.1021/acs.jpca.2c07999

Notes

The authors declare no competing financial interest.

ACKNOWLEDGMENTS

Parts of this project were generously supported by the Smithsonian Scholarly Studies Award and the Smithsonian's Museum Conservation Institute Federal Funds. G.A.N. would like to thank Ikumi Kayama for measuring the thermal paper images. C.L.-A. would like to acknowledge NSF Grant CMI 1904879 and Grant CBET 2105929.

■ REFERENCES

- (1) Takats, Z.; Wiseman, J. M.; Gologan, B.; Cooks, R. G. Mass spectrometry sampling under ambient conditions with desorption electrospray ionization. *Science* **2004**, *306*, 471–473.
- (2) Cody, R. B.; Laramee, J. A.; Durst, H. D. Versatile new ion source for the analysis of materials in open air under ambient conditions. *Anal. Chem.* **2005**, *77*, 2297–2302.
- (3) Smoluch, M.; Mielczarek, P.; Silberring, J. Plasma-based ambient ionization mass spectrometry in bioanalytical sciences. *Mass Spectrom. Rev.* **2016**, *35*, 22–34.
- (4) Martinez-Jarquin, S.; Winkler, R. Low-temperature plasma (LTP) jets for mass spectrometry (MS): Ion processes, instrumental set-ups, and application examples. *TrAC, Trends Anal. Chem.* **2017**, *89*, 133–145.
- (5) Kiontke, A.; Holzer, F.; Belder, D.; Birkemeyer, C. The requirements for low-temperature plasma ionization support miniaturization of the ion source. *Anal. Bioanal. Chem.* **2018**, *410*, 3715–3722.
- (6) Newsome, G. A. Extending the Reach: Non-Proximate Sampling for Mass Spectrometry Analysis of Large Objects and Surfaces; LCGC North America, 2021; Vol. 39.
- (7) Jones, E. A.; Simon, D.; Karancsi, T.; Balog, J.; Pringle, S. D.; Takats, Z. Matrix assisted rapid evaporation ionization mass spectrometry. *Anal. Chem.* **2019**, *91*, 9784–9791.
- (8) Funke, S. K.; Brückel, V. A.; Weber, M.; Lützen, E.; Wolf, J. C.; Haisch, C.; Karst, U. Plug-and-play laser ablation-mass spectrometry for molecular imaging by means of dielectric barrier discharge ionization. *Anal. Chim. Acta* **2021**, *1177*, No. 338770.
- (9) Rankin-Turner, S.; Turner, M. A.; Kelly, P. F.; King, R. S. P.; Reynolds, J. C. Transforming presumptive forensic testing: in situ identification and age estimation of human bodily fluids. *Chem. Sci.* **2019**, *10*, 1064–1069.

- (10) Haapala, M.; Teppo, J.; Ollikainen, E.; Kiiski, I.; Vaikkinen, A.; Kauppila, T. J.; Kostiainen, R. Solvent Jet Desorption Capillary Photoionization-Mass Spectrometry. *Anal. Chem.* **2015**, *87*, 3280–3285.
- (11) Winter, G. T.; Wilhide, J. A.; LaCourse, W. R. Molecular Ionization-Desorption Analysis Source (MIDAS) for Mass Spectrometry: Thin-Layer Chromatography. *J. Am. Soc. Mass Spectrom.* **2016**, *27*, 352–358.
- (12) Haapala, M.; Pól, J.; Saarela, V.; Arvola, V.; Kotiaho, T.; Ketola, R. A.; Franssila, S.; Kauppila, T. J.; Kostiainen, R. Desorption atmospheric pressure photoionization. *Anal. Chem.* **2007**, *79*, 7867–7872.
- (13) Chernetsova, E. S.; Revelsky, A. I.; Morlock, G. E. Some new features of Direct Analysis in Real Time mass spectrometry utilizing the desorption at an angle option. *Rapid Commun. Mass Spectrom.* **2011**, 25, 2275–2282.
- (14) Shelley, J. T.; Wiley, J. S.; Hieftje, G. M. Ultrasensitive Ambient Mass Spectrometric Analysis with a Pin-to-Capillary Flowing Atmospheric-Pressure Afterglow Source. *Anal. Chem.* **2011**, *83*, 5741–5748.
- (15) Newsome, G. A.; Kayama, I.; Brogdon-Grantham, S. A. Direct analysis in real time mass spectrometry (DART-MS) of discrete sample areas without heat damage. *Anal. Methods* **2018**, *10*, 1038–1045.
- (16) Curtis, M.; Keelor, J. D.; Jones, C. M.; Pittman, J. J.; Jones, P. R.; Sparkman, O. D.; Fernandez, F. M. Schlieren visualization of fluid dynamics effects in direct analysis in real time mass spectrometry. *Rapid Commun. Mass Spectrom.* **2015**, *29*, 431–439.
- (17) Costa, A. B.; Cooks, R. G. Simulation of atmospheric transport and droplet-thin film collisions in desorption electrospray ionization. *Chem. Commun.* **2007**, *38*, 3915–3917.
- (18) Costa, A. B.; Cooks, R. G. Simulated splashes: Elucidating the mechanism of desorption electrospray ionization mass spectrometry. *Chem. Phys. Lett.* **2008**, 464, 1–8.
- (19) Fincher, J. A.; Korte, A. R.; Reschke, B.; Morris, N. J.; Powell, M. J.; Vertes, A. Enhanced sensitivity and metabolite coverage with remote laser ablation electrospray ionization-mass spectrometry aided by coaxial plume and gas dynamics. *Analyst* **2017**, *142*, 3157–3164.
- (20) Habe, T. T.; Morlock, G. E. Quantitative surface scanning by Direct Analysis in Real Time mass spectrometry. *Rapid Commun. Mass Spectrom.* **2015**, *29*, 474–484.
- (21) Häbe, T. T.; Morlock, G. E. Improved desorption/ionization and ion transmission in surface scanning by direct analysis in real time mass spectrometry. *Rapid Commun. Mass Spectrom.* **2016**, *30*, 321–332.
- (22) Harper, J. D.; Charipar, N. A.; Mulligan, C. C.; Zhang, X.; Cooks, R. G.; Ouyang, Z. Low-Temperature Plasma Probe for Ambient Desorption Ionization. *Anal. Chem.* **2008**, *80*, 9097–9104.
- (23) Upton, K. T.; Schilling, K. A.; Beauchamp, J. L. Easily fabricated ion source for characterizing mixtures of organic compounds by direct analysis in real time mass spectrometry. *Anal. Methods* **2017**, *9*, 5065–5074.
- (24) Martínez-Jarquín, S.; Moreno-Pedraza, A.; Guillén-Alonso, H.; Winkler, R. Template for 3D printing a low-temperature plasma probe. *Anal. Chem.* **2016**, *88*, 6976–6980.
- (25) Benassi, M.; Garcia-Reyes, J. F.; Spengler, B. Ambient ion/molecule reactions in low-temperature plasmas (LTP): reactive LTP mass spectrometry. *Rapid Commun. Mass Spectrom.* **2013**, *27*, 795–804. (26) Cody, R. B.; Dane, A. J. Dopant-assisted direct analysis in real
- (26) Cody, R. B.; Dane, A. J. Dopant-assisted direct analysis in real time mass spectrometry with argon gas. *Rapid Commun. Mass Spectrom.* **2016**, 30, 1181–1189.
- (27) Lei, Y. T.; Lu, Y.; Zhang, T. C.; Qi, Y.; Lu, Y. F. Rapid screening of testosterone in the aquatic environment using direct analysis in real-time (DART) mass spectrometry. *Environ. Earth Sci.* **2016**, 75, 1.
- (28) Ninomiya, S.; Shimada, H.; Kinoshita, K.; Rankin-Turner, S.; Hiraoka, K. Heat Pulse Desorption of Low-Volatility Compounds by a Heated N2 Gas Pulse with Mass Spectrometry. *J. Am. Soc. Mass Spectrom.* **2022**, 33, 2046–2054.
- (29) Ellis, W. C.; Lewis, C. R.; Openshaw, A. P.; Farnsworth, P. B. The Effects of Added Hydrogen on Noble Gas Discharges Used as Ambient

Desorption/Ionization Sources for Mass Spectrometry. J. Am. Soc. Mass Spectrom. **2016**, 27, 1539–1549.

- (30) Song, L.; Chuah, W. C.; Lu, X.; Remsen, E.; Bartmess, J. E. Ionization Mechanism of Positive-Ion Nitrogen Direct Analysis in Real Time. *J. Am. Soc. Mass Spectrom.* **2018**, *29*, 640–650.
- (31) Su, R.; Yu, W.; Sun, K.; Yang, J.; Chen, C.; Lian, W.; Liu, S.; Yang, H. The Ion Source of Nitrogen Direct Analysis in Real-Time Mass Spectrometry as a Highly Efficient Reactor: Generation of Reactive Oxygen Species. *J. Am. Soc. Mass Spectrom.* **2019**, *30*, 581–587.
- (32) Newsome, G. A.; Kavich, G.; Alvarez-Martin, A. Interface for Reproducible, Multishot Direct Analysis of Solid-Phase Microextraction Samples. *Anal. Chem.* **2020**, *92*, 4182–4186.

□ Recommended by ACS

Chemical Imaging of Organic Materials by MeV SIMS Using a Continuous Collimated Ion Beam

Zdravko Siketić, Marijana Popović Hadžija, et al.

JANUARY 27, 2023

ANALYTICAL CHEMISTRY

READ 🗹

Transforming a Mid-infrared Laser Profile from Gaussian to a Top-Hat with a Diffractive Optical Element for Mass Spectrometry Imaging

Hongxia Bai, David C. Muddiman, et al.

DECEMBER 21, 2022

JOURNAL OF THE AMERICAN SOCIETY FOR MASS SPECTROMETRY

READ 🗹

A Comparison of the Performance of Modular Standalone Do-It-Yourself Ion Mobility Spectrometry Systems

Cameron N. Naylor, Brian H. Clowers, et al.

MARCH 14, 2023

JOURNAL OF THE AMERICAN SOCIETY FOR MASS SPECTROMETRY

READ 🗹

Field-Gradient-Focusing Ion Guide for Enhanced Transfer Efficiency of Low-Mass Ions

Shiyu Du, Yanbing Zhai, et al.

JANUARY 11, 2023

ANALYTICAL CHEMISTRY

READ 🗹

Get More Suggestions >